Simulation of wave run-up by means of the exact solution of the wet/dry Riemann problem

MARCO TAMBURRINO, GIOVANNI CANNATA
Department of Civil, Constructional and Environmental Engineering
"Sapienza" University of Rome
Via Eudossiana 18 – 00184, Rome
ITALY
marco.tamburrino@uniroma1.it

Abstract: - An innovative method for the simulation of the hydrodynamics in the swash zone, related to the wave run-up phenomenon, is presented. This method applies the exact solution of the Riemann problem over a dry bed to correctly evaluate the celerity of water waves propagating over the shore, and so to precisely track the coastline location. The simulations of velocity and wave fields outside the surf zone, inside the surf zone and in the swash zone, are carried out by means of a numerical model which solves 3D motion equations expressed in integral form, with a vertical coordinate that varies in time in order to follow the free surface evolution. Several numerical validation tests are carried out, in order to verify the capability of the method to track the coastline.

Key-Words: - wave run-up, wet-dry, Riemann problem, time-varying coordinates, free-surface

1 Introduction

One of the most important hydrodynamics phenomena that occurs in coastal regions is the wave run-up, that is the phenomenon described by the backward and forward motion of the wave front that separates the wet zone and the dry zone. A proper evaluation of the wave run-up is necessary in order to predict the nearshore currents related to wave trains.

In this context, numerical models based on depth-averaged motion equations, such as Nonlinear Shallow Water Equations or Boussinesq Equations, are used extensively [1-6]. In particular, the models that solve Boussinesq Equations are capable to simulate wave transformation from deep to shallow water, unlike models based on Nonlinear Shallow Water Equations.

A number of numerical models in literature solves the three-dimensional Navier-Stokes Equations, which can be integrated over structured [7] or unstructured grids [8,9]. The most immediate advantage of this kind of models is that they can predict the vertical distribution of the flow variables, unlike models that solve depth-averaged equations. In the context of models that solve the three-dimensional Navier-Stokes Equations for free surface flows, one of the most challenging issues is the free surface tracking. The Volume of Fluid (VOF) technique is one of the most employed methods to locate free surface [10,11]. The main drawback of the VOF technique is the difficulty to precisely assign pressure and kinematic boundary conditions at the free surface, given the fact that the vertical fluxes cross the computational cells arbitrarily.

Many recent 3D models use the so-called σ-coordinate transformation [7,12-14]. By means of this transformation, the physical domain, that varies over time with the free surface variation, is mapped into a fixed rectangular prismatic shape computational grid. By means of these models, the free surface position is at the upper computational boundary, so that kinematic and zero-pressure conditions at the free-surface are assigned precisely.

In the context of nearshore coastal flows, a proper numerical simulation of the wave run-up in the swash zone is fundamental. The nearshore wave currents related to the propagation of waves in the swash zone substantially influence the bed erosion e the bed and coastline evolution. For this reason, it is very important to carefully locate the coastline position over time. In order to identify such position, an esteem of the celerity of the wave front that divides the wet zone and the dry zone, is necessary. The proper detection of the coastline in the swash zone represents a challenging issue. In fact, the celerity of the wet/dry wave front is often badly evaluated by the existing methods.

One of the most used techniques in literature to evaluate the advance of the wet/dry wave front, is the so-called thin film technique [15]. By means of this technique, the zone in which the fluid is absent

(the dry zone), is assumed to be covered by a thin layer of water. The wet/dry front celerity is evaluated by solving a Riemann problem (an initial value problem with piecewise constant initial data separated by a discontinuity, in the context of a systems of hyperbolic equations) whose initial data are always defined by wet zones. Unfortunately, solving a Riemann problem in wet conditions lead to an error in the calculation of the wet-dry wave front celerity.

The WAF (Weighted Average Flux) method is applied to the detection of the wet/dry front by [16]. By means of this method, the volume of water that crosses the interface (which defines the position of the coastline) between the last wet calculation cell and the first dry calculation cell, is evaluated; when this volume exceeds a threshold value a priori defined, the dry calculation cell becomes wet and the wet/dry front moves to the new interface. This method does not evaluate directly the wet/dry wave front celerity and the esteem of such celerity depends on the threshold value choice.

In order to overcome the limitations of the models presented in literature, in this work we present a novel method for the prediction of the wave run-up, in the context of a numerical model for the free surface flow simulation, which solves an integral form of three-dimensional Navier-Stokes equations, with a vertical coordinate that varies in time in order to follow the free surface evolution [17]. The proposed method uses the exact solution of the Riemann problem over a dry bed, in order to evaluate the wet/dry wave front celerity in a physically based way, and an iterative procedure for the evaluation of the advance over time of the wet/dry front.

The paper is structured as follows: in Chapter 2, we briefly describe the 3D numerical model that we used to simulate hydrodynamic fields in the coastline zone; in Chapter 3, we describe the exact solution of the Riemann problem over dry bed and we present an original method for the evaluation of the wet/dry wave front celerity; in Chapter 4, we present the results of several validation tests for the proposed method; in Chapter 5, we present the conclusions of the study.

2 3D numerical model

In this section, we briefly describe the numerical model that we used to simulate the hydrodinamic fields in the different zones domain (outside the surf zone, inside the surf zone and in the swash zone). The model is based on the solution an integral form of the three-dimensional Navier-Stokes equations, with a time-varying vertical coordinate. For details about the model, see [7].

Let us introduce a particular transformation from a system of Cartesian coordinates (x^1, x^2, x^3, t), to a system of curvilinear coordinates $(\xi^1, \xi^2, \xi^3, \tau)$, in which the vertical coordinate vary in time in order to follow the free surface movements:

$$\xi^1 = x^1; \quad \xi^2 = x^2; \quad \xi^3 = \frac{x^3 + h}{H}; \quad \tau = t \qquad (1)$$

In eqn. (1), H is the total water depth, h is the still water depth and η is the free surface elevation. The following relation is valid

$$H(x^1, x^2, t) = h(x^1, x^2, t) + \eta(x^1, x^2, t) \qquad (2)$$

Let (u_1, u_2, u_3) be the Cartesian components of the fluid velocity vector $\vec{u}$, and (v_1, v_2, v_3) be the Cartesian components of the velocity vector of the control volume surfaces, $\vec{v}$. Let $\vec{g}_l$ and $\vec{g}^l$ $(l = 1,2,3)$ be the covariant base vectors and the contravariant base vectors, respectively. Let $\sqrt{g}$ be the Jacobian of the transformation defined by eqn. (1). Further details on definitions can be found in [7].

Let $\Delta V(t)$ be a volume element defined by surface elements bounded by curves lying on the coordinate lines. We define the volume element in the physical space as:

$$\Delta V(t) = \Delta x^1 \Delta x^2 \Delta x^3 = \sqrt{g} \Delta \xi^1 \Delta \xi^2 \Delta \xi^3 \qquad (3)$$

and the volume element in the transformed space as:

$$\Delta V^* = \Delta \xi^1 \Delta \xi^2 \Delta \xi^3 \qquad (4)$$

$\Delta \xi^1$, $\Delta \xi^2$ and $\Delta \xi^3$ represent the volume element dimensions in the transformed space, in ξ^1, ξ^2 and ξ^3 coordinates, respectively. Similarly, we define the surface element which bounds ΔV, in the physical space as $\Delta A(t) = \Delta x^\alpha \Delta x^\beta = \sqrt{g} \Delta \xi^\alpha \Delta \xi^\beta$ and in the transformed space as $\Delta A^* = \Delta \xi^\alpha \Delta \xi^\beta$ $(\alpha, \beta = 1,2,3$ are cyclic).

By means of the coordinate transformation defined by eqn. (1), the time-varying coordinates of the physical domain are basically mapped into a fixed coordinate system (ξ^1, ξ^2, ξ^3), where ξ^3 spans from 0 to 1.

Let us define the cell averaged value, respectively of the variable Hu_l $(l = 1,2,3)$ and of

the variable H (recalling that H does not depend on ξ^3):

$$\overline{Hu_l} = \frac{1}{\Delta V^*}\int_{\Delta V^*} Hu_l d\xi^1 d\xi^2 \, d\xi^3 \tag{5}$$

$$\overline{H} = \frac{1}{\Delta A^*_{x^1x^2}}\int_{\Delta A^*_{x^1x^2}} H d\xi^1 d\xi^2 \tag{6}$$

where $\Delta A^*_{x^1x^2} = \Delta\xi^1\Delta\xi^2$ is the horizontal surface element in the transformed space.

By using eqn. (5), the integral form of the momentum equation over the volume ΔV, expressed in the time dependent coordinate system defined in (1), can be written as follows (see [7]):

$$\begin{aligned}\frac{\partial\overline{Hu_l}}{\partial\tau} = &-\frac{1}{\Delta V^*}\sum_{\alpha=1}^{3}\\ &\left\{\int_{\Delta A^{*\alpha+}}[u_l(u_m - v_m)g^\alpha_m H]d\xi^\beta d\xi^\gamma\right.\\ &\left.-\int_{\Delta A^{*\alpha-}}[u_l(u_m - v_m)g^\alpha_m H]d\xi^\beta d\xi^\gamma\right\}\\ &-\frac{1}{\Delta V^*}\sum_{\alpha=1}^{3}\left\{\int_{\Delta A^{*\alpha+}}[G\eta g^\alpha_m H]d\xi^\beta d\xi^\gamma\right.\\ &\left.-\int_{\Delta A^{*\alpha-}}[G\eta g^\alpha_m H]d\xi^\beta d\xi^\gamma\right\}\\ &-\frac{1}{\Delta V^*}\frac{1}{\rho}\int_{\Delta V^*}\frac{\partial q}{\partial\xi^\alpha}g^\alpha_m H d\xi^1 d\xi^2 d\xi^3\\ &-\frac{1}{\Delta V^*}\sum_{\alpha=1}^{3}\left\{\int_{\Delta A^{*\alpha+}}[2\nu S_{lm}g^\alpha_m H]d\xi^\beta d\xi^\gamma\right.\\ &\left.-\int_{\Delta A^{*\alpha-}}[2\nu S_{lm}g^\alpha_m H]d\xi^\beta d\xi^\gamma\right\}\end{aligned} \tag{7}$$

where $\Delta A^{*\alpha+}$ and $\Delta A^{*\alpha-}$ indicate the boundary surfaces of the volume element ΔV^* on which ξ^α is constant and which are located at the larger and the smaller value of ξ^α, respectively. Here the indexes α, β and γ are cyclic. In eqn. (7) G is the constant of gravity, ρ is the fluid density, q is the dynamic pressure, ν is the kinematic viscosity and S_{lm} is the strain rate tensor.

By using eqn. (6), the integral form of continuity equation over the water column, expressed in the time dependent coordinate system defined in (1), can be written as follows (see [7]):

$$\begin{aligned}\frac{\partial\overline{H}}{\partial\tau} + \frac{1}{\Delta A^*_{x^1x^2}}\int_0^1\sum_{\alpha=1}^{2}\left[\int_{\Delta\xi^{\alpha+}} Hu_\alpha d\xi^\beta\right.\\ \left.-\int_{\Delta\xi^{\alpha-}} Hu_\alpha d\xi^\beta\right]d\xi^3 = 0\end{aligned} \tag{8}$$

in which $\xi^{\alpha+}$ and $\xi^{\alpha-}$ indicate the boundary lines of the surface element ΔA^* on which ξ^α is constant and which are located at the larger and the smaller value of ξ^α respectively. Eqn. (8) represents the governing equation that predicts the free surface motion.

Eqns. (7) and (8) represent the expression of the three dimensional motion equations as a function of the $\overline{Hu_l}$ and $\overline{H}$ variables in the coordinate system $(\xi^1, \xi^2, \xi^3, \tau)$. Eqns. (7) and (8) are solved by means of a numerical model whose details can be found in [7].

3 The wet-dry problem

In the simulation of the wave run-up phenomenon, a good prediction of the water wave propagation over dry beds, is essential. In particular, the scheme has to be able to simulate this propagation both over variable bathymetry and over flat beds. In order to simulate the run-up and the backwash dynamics of the wet and dry front in the swash zone, the following original procedure is proposed.

3.1 The Riemann problem over a dry bed

In order to properly represent the celerity by means of which the wet/dry wave front propagates, let us describe the solution of Riemann problem over a dry bed.

In general, the solution of the Riemann problem consists on the solution of a system of partial differential hyperbolic equations, piecewise constant initial data separated by a discontinuity. For the sake of simplicity, let us consider the Riemann problem for the one-dimensional homogeneus Shallow Water Equations [15]:

$$\begin{cases}\dfrac{\partial H}{\partial\tau} + \dfrac{\partial(uH)}{\partial x} = 0\\ \dfrac{\partial(uH)}{\partial\tau} + \dfrac{\partial\left(Hu^2 + \frac{1}{2}GH^2\right)}{\partial x} = 0\end{cases} \tag{9}$$

With initial data:

$$u(t=0)=\begin{cases}u_L & \text{if } x<0\\ u_R & \text{if } x>0\end{cases}$$
$$H(t=0)=\begin{cases}H_L & \text{if } x<0\\ H_R & \text{if } x>0\end{cases} \quad (10)$$

The subscripts L e R indicate the initial data value on the left side and on the right side of the discontinuity, respectively. In eqn. (9), H is the water depth and u is the depth-averaged velocity.

Let us analyze the Riemann problem over a dry bed (see fig. 1), whose initial data are given by a wet state on the left side of the discontinuity ($H_L > 0$) and by a dry state on the right of the discontinuity ($H_R = H_0 = 0, u_R = u_0 = 0$).

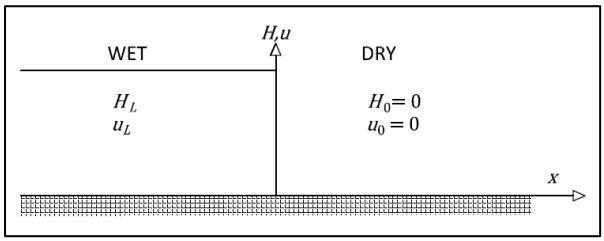

Fig. 1. Riemann problem over dry bed. Initial data values.

If the above described Riemann problem over a dry bed were solved by applying the general solution of the Riemann problem, in which $H_L > 0$ and $H_R > 0$, there would be an error. In fact, the characteristic fan for the solution with initial data $H_L > H_R > 0$ is composed by a shock wave. It can be demonstrated that in the solution of the Riemann problem in the case in which in the initial data there is a dry state ($H_L = 0$ or $H_R = 0$), a shock wave cannot be present. This demonstration is shown below.

Let us suppose the two states (H_L, u_L) and (H_R, u_R) be connected by a shock wave with celerity C. Let us introduce the Rankine-Hugoniot conditions, which describe the relationship between the solution on one side of the shock wave, and the solution on the other side, for a one-dimensional flow.

The application of the Rankine-Hugoniot conditions leads to the following system of equations [15]:

$$\begin{bmatrix} H_L u_L \\ H_L {u_L}^2 + \frac{1}{2} G {H_L}^2 \end{bmatrix} - \begin{bmatrix} H_0 u_0 \\ H_0 {u_0}^2 + \frac{1}{2} G {H_0}^2 \end{bmatrix} = C\left(\begin{bmatrix} h_L \\ h_L u_L \end{bmatrix} - \begin{bmatrix} h_0 \\ h_0 u_0 \end{bmatrix} \right) \quad (11)$$

Eqn. (11), rewritten in an extended form, reads:

$$H_L u_L = H_0 u_0 + C(H_L - H_0) \quad (12)$$

$$H_L {u_L}^2 + \frac{1}{2} G {H_L}^2 = H_0 {u_0}^2 + \frac{1}{2} G {H_0}^2 + C(H_L u_L - H_0 u_0) \quad (13)$$

By imposing that $H_0 = 0$, from eqn. (12) we obtain:

$$H_L u_L = \cancel{H_0} u_0 + C(H_L - \cancel{H_0}) \quad (14)$$

$$H_L u_L = C H_L \quad (15)$$

$$C = u_L \quad (16)$$

According to eqn. (16), the celerity of the shock wave is equal to the velocity of the particles in the left state. By imposing that $H_0 = 0$, from eqn. (13) we obtain:

$$H_L {u_L}^2 + \tfrac{1}{2} G {H_L}^2 = \cancel{H_0} {u_0}^2 + \tfrac{1}{2} G \cancel{{H_0}^2} + C(H_L u_L - \cancel{H_0} u_0) \quad (17)$$

$$H_L {u_L}^2 + \frac{1}{2} G {H_L}^2 = C H_L u_L \quad (18)$$

By applying eqn. (16) to eqn. (18), we obtain:

$$H_L {u_L}^2 + \frac{1}{2} G {H_L}^2 = H_L {u_L}^2 \quad (19)$$

$$H_L = 0 \quad (20)$$

According to eqn. (20), the initial water depth on the left of the discontinuity. This is in contradiction with the initial hypothesis according to which $H_L > 0$. Therefore, it can be assumed that a shock wave cannot separate a wet solution state from a dry solution state, hence a shock wave cannot represent a wet/dry wave front. Thus, a shock wave cannot exist in proximity of a dry zone.

Let us consider the case in which there is a left wet state and a right dry state in the initial data (as shown in fig. 2):

$$u(t=0)=\begin{cases}u_L & \text{if } x<0\\ u_R = u_0 = 0 & \text{if } x>0\end{cases}$$
$$H(t=0)=\begin{cases}H_L & \text{if } x<0\\ H_R = H_0 = 0 & \text{if } x>0\end{cases} \quad (21)$$

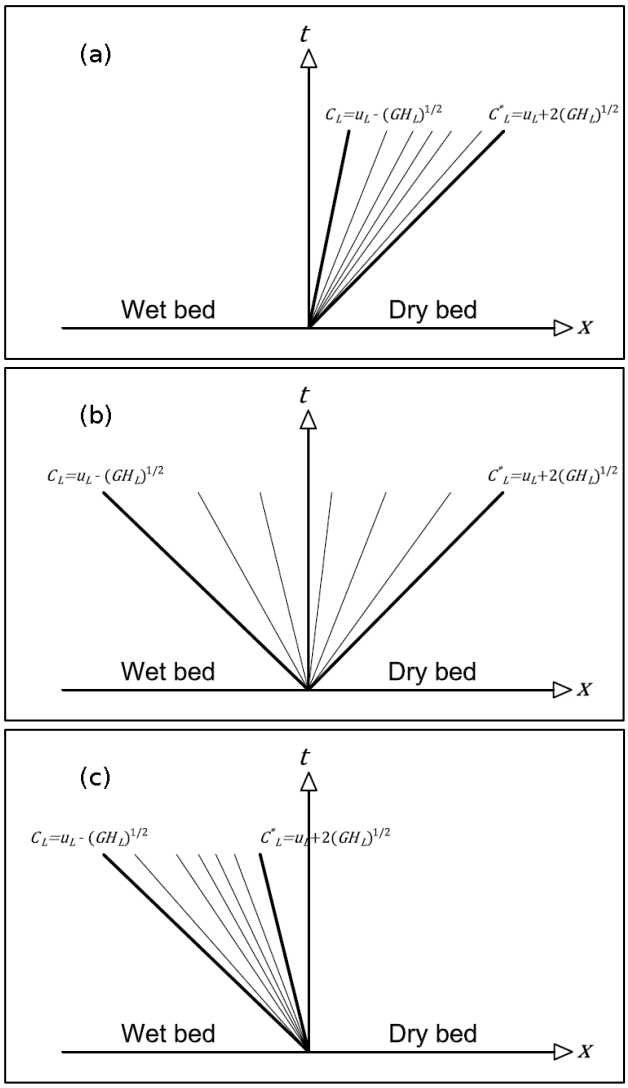

Fig. 2. Riemann problem over dry bed. Exact solution in case of:

- $u_L - \sqrt{GH_L} > 0$ and $u_L + 2\sqrt{GH_L} > 0$ (a);
- $u_L - \sqrt{GH_L} < 0$ and $u_L + 2\sqrt{GH_L} > 0$ (b);
- $u_L - \sqrt{GH_L} < 0$ and $u_L + 2\sqrt{GH_L} < 0$ (c).

In this Riemann problem configuration, a left rarefaction wave is present, related to the left eigenvalue $\lambda_1 = u - \sqrt{GH}$ (see [15]). The wave that connects the dry solution state to a wet solution state, that advances with celerity C_L^*, is the tail of the aforementioned rarefaction wave. Hence, the tail of the rarefaction wave defines the wet/dry wave front.

Let us show the complete exact solution of the Riemann problem over a dry bed. Let us consider a fluid particle that belongs to the wet/dry front. Let H_c and u_c be particle water depth and velocity, respectively. The wet dry front celerity C_L^* is given by:

$$C_L^* = \frac{dx}{dt} = u_c - \sqrt{GH_c} \tag{22}$$

Recalling that the tail of the rarefaction wave is the wet/dry wave front, we have:

$$H_c = 0 \tag{23}$$

By using eqn. (23) into eqn. (22), we have

$$C_L^* = u_c \tag{24}$$

Recalling Riemann invariants [15], it can be assumed that over the rarefaction wave the following relation is valid:

$$u + 2\sqrt{GH} = \text{cost} \tag{25}$$

By applying eqn. (25) to the head and the tail of the rarefaction wave, we have:

$$u_c + 2\sqrt{GH_c} = u_L + 2\sqrt{GH_L} \tag{26}$$

By using eqn. (23) into eqn. (26), we have

$$u_c = u_L + 2\sqrt{GH_L} \tag{27}$$

From eqns. (24) and (27), we have:

$$C_L^* = u_L + 2\sqrt{GH_L} \tag{28}$$

By means of eqn. (28), the celerity of the wet/dry front can be evaluated. The complete solution of the Riemann problem over a dry bed, is (see [15]):

$$u(x,t) = \begin{cases} u_L & \text{if } \frac{x}{t} \le u_L - \sqrt{GH_L} \\ u_{fan} & \text{if } u_L - \sqrt{GH_L} \le \frac{x}{t} \le C_L^* \\ u_R = u_0 = 0 & \text{if } \frac{x}{t} \ge C_L^* \end{cases}$$
$$H(x,t) = \begin{cases} H_L & \text{if } \frac{x}{t} \le u_L - \sqrt{GH_L} \\ H_{fan} & \text{if } u_L - \sqrt{GH_L} \le \frac{x}{t} \le C_L^* \\ H_R = H_0 = 0 & \text{if } \frac{x}{t} \ge C_L^* \end{cases} \tag{29}$$

Where the solution inside the rarefaction fan is given by:

$$H_{fan} = \frac{1}{G}\sqrt{\frac{1}{3}\left(u_L + 2\sqrt{GH_L} - \frac{x}{t}\right)} \tag{30}$$

$$u_{fan} = \frac{1}{3}\left(u_L + 2\sqrt{GH_L} + \frac{2x}{t}\right) \tag{31}$$

3.2 Evaluation of the advance of the wet/dry wave front

In this subsection, we describe the procedure by means of which the wet/dry wave front is advanced. For the sake of simplicity, the procedure is described for the only ξ^1 direction, by neglecting the ξ^2 direction. Let be (i,k) the two indexes which define the center of the calculation cells in the ξ^1 and ξ^3 directions, respectively. Hereinafter, the superscript (n) indicates the time level τ^n of the known variables, while the superscript $(n+1)$ indicates the time level $\tau^{n+1} = \tau^n + \Delta\tau$, of the unknown variables (see [7]).

Let us define the wet column I_i as the set of calculation cells stacked on top of each other, characterized by the same i index and by having $H_i > H_{min}$. A dry column differs from a wet column because in a dry column $H_i < H_{min}$. A dry column can change status to wet only if at least one of the adjacent columns is wet. Let be I_i a dry column and I_{i-1} a wet column. The criterion by means of which I_i changes status from dry to wet is described as follows.

Asymmetric WENO reconstructions defined on the wet column I_{i-1} lead to the evaluation of the point-value variables $H^{(n)-}_{i-1/2}$ and $u_1{}^{(n)-}_{i-1/2,k}$ located at the cell faces. In the dry column I_i, reconstructions are not carried out, and point-values variables $H^{(n)+}_{i-1/2}$ and $u_1{}^{(n)+}_{i-1/2,k}$ are set to zero.

In order to use the solution of the one-dimensional Riemann problem described in subsection 3.1, the depth-averaged velocity value has to be evaluated. For this reason, we evaluate the average over ξ^3 of $u_1{}^{(n)-}_{i-1/2,k}$ values at the interface between the column I_{i-1} and the column I_i, to obtain the depth-averaged velocity values $\breve{u}_1{}^{(n)}_{i-1/2}$:

$$\breve{u}_1{}^{(n)}_{i-1/2} = \sum_{k=1}^{m_k} \Delta\xi^3_{i-1/2,k}\, u_1{}^{(n)-}_{i-1/2,k} \tag{32}$$

In (32), m_k is the number of cells in the column and $\Delta\xi^3_{i-1/2,k} = \left(\xi^3_{i-1/2,k+1/2} - \xi^3_{i-1/2,k-1/2}\right)$.

By means of eqn. (28), the propagation celerity of the wet-dry front $\breve{C}^{(n)}_{i-1/2}$ can be evaluated as the celerity of the tail of the rarefaction wave, which divides wet status from the dry status:

$$\breve{C}^{(n)}_{i-1/2} = \breve{u}_1{}^{(n)-}_{i-1/2} + 2\left(GH^{(n)-}_{i-1/2}\right)^{1/2} \tag{33}$$

Let $H^{(n+1)\star}_{i-1/2}$ and $u^{(n+1)\star}_{i-1/2}$ be the solutions of the Riemann problem over a dry bed, described in subsection 3.1, evaluated over the interface between the wet column, I_{i-1}, and the dry column, I_i. From eqn. (29), we can have three cases.

In the first case, both the celerity of the head of the wave rarefaction and the celerity of the tail of the wave rarefaction are positive (fig. 2a). From eqn. (29), we have:

$$\begin{aligned} u_1{}^{(n)-}_{i-1/2} &\geq \sqrt{GH^{(n)-}_{i-1/2}} \\ H^{(n+1)\star}_{i-1/2} &= H^{(n)-}_{i-1/2} \\ u_1{}^{(n+1)\star}_{i-1/2} &= u_1{}^{(n)-}_{i-1/2} \end{aligned} \tag{34}$$

In the second case, the celerity of the head of the wave rarefaction is negative and the celerity of the tail of the wave rarefaction is positive (fig. 2b). It must be noted that the solution is evaluated at the column interface, that is the point in which there is the discontinuity in the initial data, hence, in eqns. (30) and (31), $x = 0$. From eqns. (29), (30) and (31), we have:

$$\begin{aligned} -2\sqrt{GH^{(n)-}_{i-1/2}} \leq u_1{}^{(n)-}_{i-1/2} &\leq \sqrt{GH^{(n)-}_{i-1/2}} \\ H^{(n+1)\star}_{i-1/2} &= \frac{1}{G}\left\{\frac{1}{3}\left[u_1{}^{(n)-}_{i-1/2} + 2\sqrt{GH^{(n)-}_{i-1/2}}\right]\right\}^{1/2} \\ u_1{}^{(n+1)\star}_{i-1/2} &= \frac{1}{3}\left[u_1{}^{(n)-}_{i-1/2} + 2\sqrt{GH^{(n)-}_{i-1/2}}\right] \end{aligned} \tag{35}$$

In the third case, both the celerity of the head of the wave rarefaction and the celerity of the tail of the wave rarefaction are negative (fig. 2c). From eqn. (29), we have:

$$u_{1_{i-1/2}}^{(n)-} \leq -2\sqrt{GH_{i-1/2}^{(n)-}}$$

$$H_{i-1/2}^{(n+1)\star} = 0 \tag{36}$$

$$u_{1_{i-1/2}}^{(n+1)\star} = 0$$

Let $db^{1}{}_{i-1/2}^{(n+1)}$ be the distance between the wet-dry front and the interface between the columns I_{i-1} and I_i interface. This distance is given by:

$$db^{1}{}_{i-1/2}^{(n+1)} = \check{C}_{i-1/2}^{(n)} \cdot \Delta\tau + db^{1}{}_{i-1/2}^{(n)} \tag{37}$$

In eqn. (37), $\Delta\tau$ is the time step $\Delta\tau = \tau^{n+1} - \tau^{n}$. The criterion to decide if the column I_i changes status from dry to wet is:

$$db^{1}{}_{i-1/2}^{(n+1)} > \Delta\xi^{1} \tag{38}$$

where $\Delta\xi^{1} = \xi_{i+1/2}^{1} - \xi_{i-1/2}^{1}$ is the distance between the wet/dry wave front and the interface between the I_{i-1} and I_i columns.

The iterative procedure for the evaluation of the wet/dry wave front position, is described as follows:

1. Evaluation of the point-value variables $H_{i-1/2}^{(n)-}$ and $u_{1_{i-1/2,k}}^{(n)-}$ at the interface between the I_{i-1} and I_i columns, by means of asymmetric WENO reconstructions.
2. Evaluation of the depth-averaged velocity value $\breve{u}_{1_{i-1/2}}^{(n)}$ from point-value variables $u_{1_{i-1/2,k}}^{(n)-}$.
3. Evaluation of the wet/dry wave front celerity $\check{C}_{i-1/2}^{(n)}$ by means of eqn. (33).
4. Advancing in time at the interface between the I_{i-1} and I_i columns of the depth-averaged values, by means of the exact solution of the Riemann problem over a dry bed, by means of eqns. (34), (35), (36), to obtain $H_{i-1/2}^{(n+1)\star}$ and $u_{1_{i-1/2}}^{(n+1)\star}$.
5. Evaluation of the distance between the wet/dry wave front and the interface between the I_{i-1} and I_i columns, $db^{1}{}_{i-1/2}^{(n+1)}$, by means of eqn. (37).
6. Update of the cell averaged values $\bar{u}_1{}^{(n+1)}$ and $\bar{H}^{(n+1)}$ in the whole domain, by means of the numerical scheme, proposed by [7].
7. Check of the condition (38) for the wetting of the column I_i. If condition (38) is not satisfied, return to step 1. If condition (38) is satisfied, the column I_i becomes wet, the new wet/dry interface is located between the column I_i and the column I_{i+1}, $db^{1}{}_{i+1/2}^{(n+1)} = 0$ and return to step 1.

The described criterion is applied analogously to direction ξ^2.

4 Results and discussion

4.1 Solitary wave on a slope beach test

In order to validate the proposed method for the evaluation of the wet-dry front position, we present the results of the simulation of a solitary wave in a channel with a slope beach. Results obtained by the proposed numerical model are compared against the experimental results obtained by [18].

The test consist in the propagation of a solitary wave over a slope beach. The still water depth is $h = 0.29$ m, the wave amplitude is 0.0812 m, the beach slope is $1/20$ and the wave is generated 3.00 m far from the toe of the beach. For the numerical simulation, we adopted a minimum water depth $H_{min} = 0.001$ m.

Fig. 3 shows the comparison between numerical results obtained by the proposed model and experimental measurement obtained by [18]. Results are shown in terms of quantities normalized by still water depth, at different time instants (normalized by $\sqrt{Gh}$). Figs. 3a and 3b show the wave transformation and breaking due to the bottom change; it can be seen that both wave steepening and wave breaking are well simulated by the proposed numerical model. In Figs. 3c and 3d, the wave front is shown propagating over the beach; it can be noted that the proposed numerical wet-dry technique is able to well predict the wave front celerity over the dry bed and the maximum run-up position. From Figs. 3e, 3f and 3g, it can be seen that even the wave run-down phenomenon is very well predicted by the numerical model. The numerical results are generally in a very good agreement with the experimental measurements.

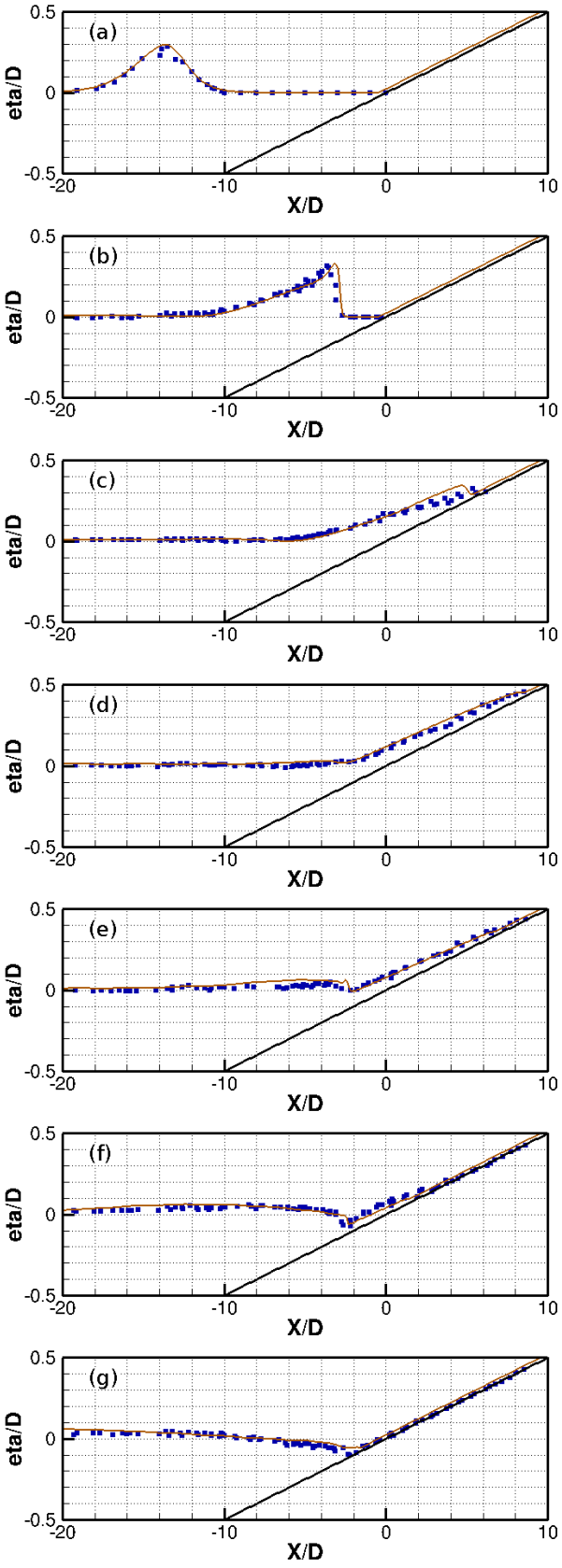

Fig. 3. Solitary wave on a slope beach. Normalized free surface elevation at: $t/\sqrt{Gh} = 10$ (a), $t/\sqrt{Gh} = 20$ (b), $t/\sqrt{Gh} = 30$ (c), $t/\sqrt{Gh} = 40$ (d), $t/\sqrt{Gh} = 50$ (e), $t/\sqrt{Gh} = 60$ (f), $t/\sqrt{Gh} = 70$ (g). Red line: numerical results. Blue squares: experimental results by [18].

4.2 Rip current test

In order to evaluate the ability to predict run-up in the 3D context by means of the proposed method for the evaluation of the wet-dry front position, we reproduce the laboratory experiment carried out by [19].

The experimental set-up of the test carried out by [19] has the following characteristics: a 30x30m basin, a plane sloping beach of $1/30$ with a channel located along the centerline. In fig. 4, the still water depth is shown. The bathymetry is symmetric with respect to the channel axis. At the boundaries that are parallel to the x-axis, reflective boundary conditions are imposed. In this subsection, we show the results obtained by simulating a wave train generated in deep water ($X = 0\,m$) with the following features: wave period $T = 1.25\,s$, wave height $A = 0.07m$.

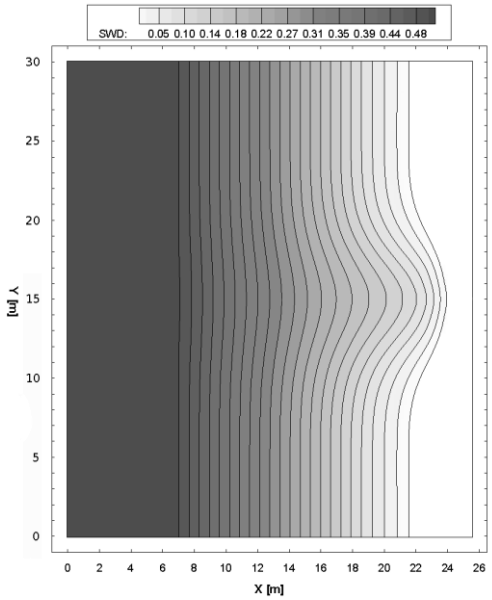

Fig. 4. Rip current test. Still water depth [m].

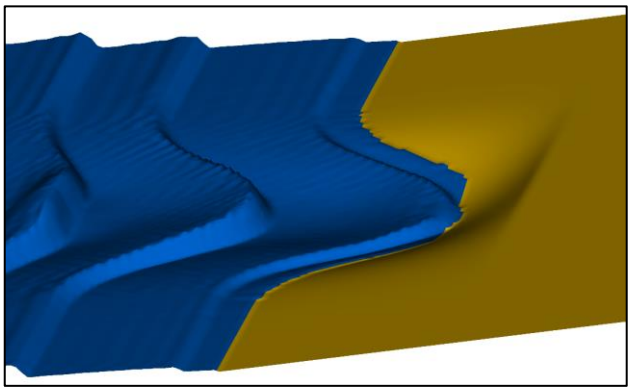

Fig. 4. Rip current test. General 3D view of water depth. Orange: dry zone. Blue: wet zone.

In fig. 5, a 3D view of the water depth is shown. Fig. 5 shows the complex wave field transformation

caused by the spatially variable bathymetry. Is to be noted the wave field propagates differently in the channel section and outside the channel. From. fig. 5, it can be seen that the model is able to properly predict all the aspects of the wave propagation from deep to shallow water, outside the surf zone, into the surf zone and into the swash zone (thanks also to the proposed wet/dry front detection method).

Fig. 6 shows several 3D views of the water depth, with particular regard to the swash zone. Fig. 6a shows a wave front at the start of the run-up phase in the channel zone. Fig. 6b shows the wet/dry wave front advancing over the beach, both in the channel and outside the channel. In fig. 6c, the wet-dry wave front is shown to have reached the maximum run-up in the channel, while yet advancing outside the channel. Fig. 6d shows the wave run-down at the center of the channel, while outside the channel the wet/dry front reaches the maximum run-up. Fig. 6e shows that outside the channel the wet/dry wave front moves backward, while in the channel another wave front is advancing. From figs. 6c, 6d and 6e, it can be seen that the proposed wet/dry front detection method is capable to handle spatially complex problems, in which there is a substantial difference, in the run-up phenomenon, among different zones of the domain. In fig. 6f, a new run-up phase is displayed, showing that the proposed model is capable to track the wet/dry front position in case of continuous wave trains.

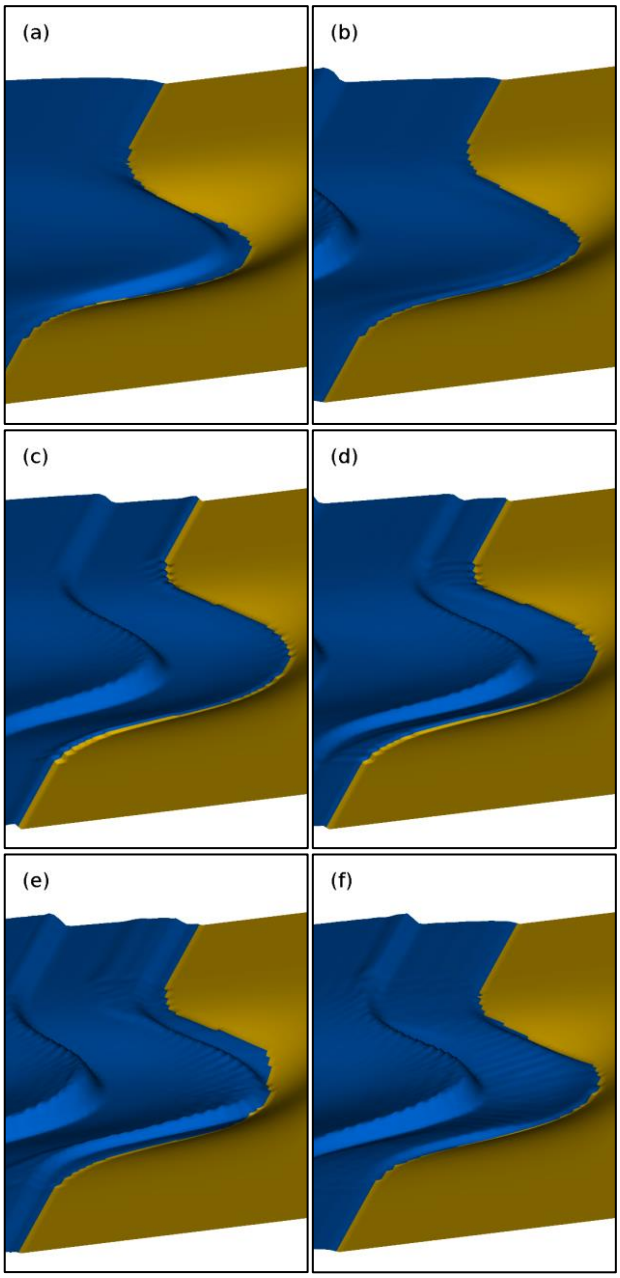

Fig. 6. Rip current test. 3D view of water depth in the swash zone at: t = 39 s (a), t = 39.33 s (b), t = 39.67 s (c), t = 40 s (d), t = 40.33 s (e), t = 40.67 s (f). Orange: dry zone. Blue: wet zone.

4 Conclusion

A study of wave run-up phenomenon in the swash zone by means of an innovative method, has been presented. The proposed method is based on the exact solution of the Riemann problem over dry bed, by means of which the celerity of the wave wet/dry front is correctly evaluated; this allows the method to precisely detect the wet/dry front position. The proposed method is applied in the context of a numerical model that solves three-dimensional motion equations, expressed in integral form, in which the vertical coordinate varies in time in order to follow the free surface movement. The validation tests that were carried out showed that the proposed method for the detection of the wet/dry front, is capable to precisely evaluate the shoreline location, allowing the numerical model to correctly predict the hydrodynamics phenomena in the swash zone.

References:

[1] Cannata, G., Lasaponara, F. & Gallerano, F., Non-linear Shallow Water Equations numerical integration on curvilinear boundary-conforming grids, *WSEAS Transactions on Fluid Mechanics*, Vol.10, 2015, pp. 13–25.

[2] Gallerano, F., Cannata, G., De Gaudenzi, O. & Scarpone, S., Modeling Bed Evolution Using Weakly Coupled Phase-Resolving Wave Model and Wave-Averaged Sediment Transport

Model, *Coastal Engineering Journal*, Vol.58, No.3, 2016, pp. 1650011-1–1650011-50.

[3] Cannata, G., Petrelli, C., Barsi, L., Fratello, F. & Gallerano, F., A dam-break flood simulation model in curvilinear coordinates, *WSEAS Transactions on Fluid Mechanics*, Vol. 13, 2018, pp. 60–70.

[4] Chen, X., A fully hydrodynamic model for three-dimensional free-surface flows, *International Journal for Numerical Methods in Fluids*, Vol.42, No.9, 2003, pp. 929–952.

[5] Shi, F., Kirby, J.T., Harris, J.C., Geiman, J.D. & Grilli, S.T., A high-order adaptive time-stepping TVD solver for Boussinesq modeling of breaking waves and coastal inundation, *Ocean Modelling*, Vol.43-44, 2012, pp. 36–51.

[6] Cioffi, F. & Gallerano, G., From rooted to floating vegetal species in lagoons as a consequence of the increases of external nutrient load: An analysis by model of the species selection mechanism, *Applied Mathematical Modelling*, Vol.30, No.1, 2006, pp. 10–37.

[7] Cannata, G., Petrelli, C., Barsi, L., Camilli, F. & Gallerano, F., 3D free surface flow simulations based on the integral form of the equations of motion, *WSEAS Transactions on Fluid Mechanics*, Vol.12, 2017, pp. 166–175.

[8] Gallerano, F., Pasero, E. & Cannata, G., A dynamic two-equation Sub Grid Scale model, *Continuum Mechanics and Thermodynamics*, Vol.17, No.2, 2005, pp. 101–123.

[9] Sørensen, O.R., Schäffer, H.A. & Sørensen, L.S., Boussinesq-type modelling using an unstructured finite element technique, *Coastal Engineering*, Vol. 50, No. 4, 2004, pp. 181–198.

[10] Harlow, F.H. & Welch, J.E., Numerical Calculation of Time-Dependent Viscous Incompressible Flow of Fluid with Free Surface, *Physics of Fluids*, Vol.8, No.12, 1965, pp. 2182–2189.

[11] Bradford, S.F., Numerical Simulation of Surf Zone Dynamics, *Journal of Waterway Port Coastal and Ocean Engineering*, Vol.126, No.1, 2000, pp. 1–13.

[12] Cannata, G., Gallerano, F., Palleschi, F., Petrelli, C. & Barsi, L., Three-dimensional numerical simulation of the velocity fields induced by submerged breakwaters. *International Journal of Mechanics*, Vol.13, 2019, pp. 1–14.

[13] Ma, G., Shi, F. & Kirby, J.T., Shock-capturing non-hydrostatic model for fully dispersive surface wave processes, *Ocean Modelling*, Vol.43–44, 2012, pp. 22–35.

[14] Gallerano, F., Cannata, G., Lasaponara, F. & Petrelli, C., A new three-dimensional finite-volume non-hydrostatic shock-capturing model for free surface flow, *Journal of Hydrodynamics*, Vol.29, No.4, 2017, pp. 552–566.

[15] Toro, E., *Shock-capturing methods for free-surface shallow flows*, John Wiley and Sons, Manchester, UK, 2001.

[16] Brocchini, M., Bernetti, R., Mancinelli, A. & Albertini, G., An efficient solver for nearshore flows based on the WAF method. *Coastal Engineering*, Vol.43, 2001, pp. 105–129

[17] Cannata, G., Petrelli, C., Barsi, L. & Gallerano F., Numerical integration of the contravariant integral form of the Navier-Stokes equations in time-dependent curvilinear coordinate system for three-dimensional free surface flows, *Continuum Mechanics and Thermodynamics*, Vol.31, No.2, 2019, pp.491–519.

[18] Synolakis, C.E., The runup of solitary waves, *Journal of Fluid Mechanics*, Vol.185, 1987, pp. 523–545.

[19] Hamm, L., Directional nearshore wave propagation over a rip channel: an experiment, *Proceedings of the 23rd International Conference of Coastal Engineering*, 1992.